Dynamics of Sheared Convective Boundary Layer Entrainment. Part II: Evaluation of Bulk Model Predictions of Entrainment Flux

ROBERT J. CONZEMIUS*

School of Meteorology, University of Oklahoma, Norman, Oklahoma, and Department of Atmospheric Science, Colorado State University, Fort Collins, Colorado

EVGENI FEDOROVICH

School of Meteorology, University of Oklahoma, Norman, Oklahoma

(Manuscript received 10 May 2005, in final form 17 September 2005)

ABSTRACT

Several bulk model–based entrainment parameterizations for the atmospheric convective boundary layer (CBL) with wind shear are reviewed and tested against large-eddy simulation (LES) data to evaluate their ability to model one of the basic integral parameters of convective entrainment—the entrainment flux ratio. Test results indicate that many of these parameterizations fail to correctly reproduce entrainment flux in the presence of strong shear because they underestimate the dissipation of turbulence kinetic energy (TKE) produced by shear in the entrainment zone. It is also found that surface shear generation of TKE may be neglected in the entrainment parameterization because it is largely balanced by dissipation. However, the surface friction has an indirect effect on the entrainment through the modification of momentum distribution in the mixed layer and regulation of shear across the entrainment zone. Because of this effect, parameterizations that take into account the surface friction velocity but exclude entrainment zone shear may sufficiently describe entrainment when wind shear in the free atmosphere above the CBL is small. In this case, the surface shear acts as a proxy for the entrainment zone shear. Such parameterizations can be most useful if applied in situations where atmospheric data are insufficient for calculating entrainment zone shear. The importance of modeling a Richardson-number-limited, finite-depth entrainment zone is evidenced by the relatively accurate entrainment flux predictions by models that explicitly account for effects of entrainment zone shear, but predictions by these models are often adversely affected by the underestimation of TKE dissipation in the entrainment zone.

1. Introduction

The daytime atmospheric convective boundary layer (CBL) is the turbulent lower portion of the troposphere that is in contact with the earth and whose turbulence is primarily forced by positive fluxes of buoyancy from the surface. The CBL development is associated with the entrainment of free atmospheric air, from above, into the growing CBL. In the present study, which is divided into two parts, we are focusing on the entrainment in sheared, horizontally homogeneous, dry atmospheric CBLs. Conzemius and Fedorovich (2006, hereafter Part I) investigates entrainment in sheared CBLs as reproduced by large-eddy simulations (LES). In the current part, our goal will be to assess the overall ability of earlier proposed entrainment parameterizations, based on the so-called bulk model approach (Fedorovich 1998), to reproduce entrainment for the set of 24 simulated CBL cases described in Part I.

In the early studies of the atmospheric CBL entrainment (Ball 1960; Lilly 1968; Betts 1973; Carson 1973; Stull 1973; Tennekes 1973), which utilized the CBL bulk model approach (see Part I for its description), the contribution of shear-driven turbulence to the evolution of the CBL was neglected on the basis that it comprises an insignificant source of turbulence kinetic energy (TKE). In many CBL cases, this assumption is rather well justified. Besides that, leaving the shear production of TKE out of entrainment equations in bulk

* Current affiliation: Windlogics, Inc., Grand Rapids, Minnesota.

Corresponding author address: Robert J. Conzemius, Windlogics, Inc., 201 NW 4th Street, Grand Rapids, MN 55744.
E-mail: robert.conzemius@att.net

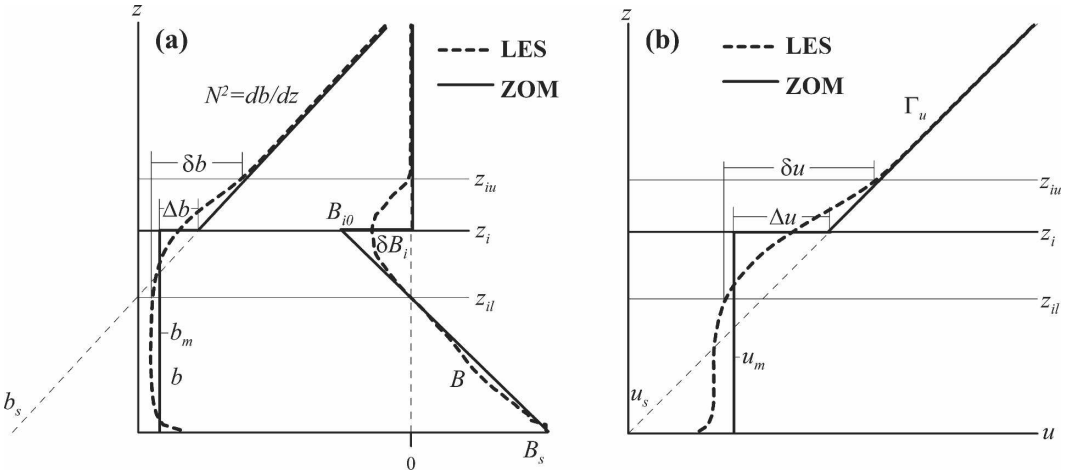

FIG. 1. Profiles of (a) buoyancy and buoyancy flux and (b) velocity in the horizontally (quasi) homogeneous CBL. Heavy dashed lines indicate LES or atmospheric horizontally averaged profiles, and heavy solid lines indicate their representation in the ZOM. Lighter solid lines are the lower (z_{il}) and upper (z_{iu}) limits of the entrainment zone. The diagonal dashed line in (b) represents the profile of geostrophic wind. For changes of any variable ϕ across the entrainment zone, $\delta\phi$ refers to the change of that variable across the entire entrainment zone, and $\Delta\phi$ refers to the change of that variable in the ZOM.

models greatly simplifies those equations, and even in this simplified form, they often describe CBL entrainment rather well. However, a purely shear-free CBL rarely exists in the atmosphere and, when the surface buoyancy flux is relatively weak and the wind shear is relatively strong, the shear effects in the CBL become significant and cannot be neglected (Stull 1976a,c; Mahrt and Lenschow 1976).

Bulk model equations (or parameterizations) that take into account the effects of shear on the TKE production and entrainment rate in atmospheric CBLs have been suggested in a number of CBL studies, the first of which date back to the mid 1970s (Tennekes 1973, hereafter T73; Mahrt and Lenschow 1976, hereafter ML76; Stull 1976a,b,c, hereafter ST76; Zeman and Tennekes 1977, hereafter ZT77; Tennekes and Driedonks 1981, hereafter TD81; Driedonks 1982, hereafter D82; Boers et al. 1984, hereafter B84; Batchvarova and Gryning 1991, 1994, hereafter BG94; Fedorovich 1995; Pino et al. 2003, hereafter P03; Sorbjan 2004, hereafter SR04; Kim et al. 2005, manuscript submitted to *Bound.-Layer Meteor.,* hereafter K05). In many cases, those parameterizations were developed based on specific CBL datasets. The overall number of sheared CBL cases investigated with bulk models is relatively small, however, and in many of them the CBL development was ultimately dominated by the buoyancy production of TKE. The current study seeks to test entrainment parameterizations for CBLs in which the shear-production of TKE is relatively strong, competing with the buoyancy production of TKE in driving the CBL development. Specifically, we seek to evaluate the physical hypotheses and assumptions that underlie the bulk model based entrainment parameterizations for sheared CBLs and to help quantify the shear enhancement of entrainment studied in Part I.

A majority of bulk approaches adopt the zero-order model (ZOM) representation of the CBL structure (Lilly 1968), which considers the entrainment zone buoyancy and velocity jumps as finite discontinuities across an infinitesimally thin interface between the convectively mixed layer and the free atmosphere (Betts 1973; Carson 1973; T73; ST76; ZT77; TD81; D82; B84; BG94; Fedorovich 1995; P03; see Fig. 1). Another popular bulk approach is based on the first-order model (FOM) of the CBL suggested by Betts (1974). In this model, the velocity and buoyancy changes in the entrainment zone are represented by linear profiles over a finite layer (ML76; K05). Some other studies, like SR04, are not specific as to the type of bulk model used but implicitly assume at least a first-order representation of the CBL structure.

These various bulk model methodologies look differently at roles played by the surface shear and entrainment zone shear in the turbulence generation and evolution of the CBL. For both shear types, an important parameter appears to be the fraction of shear-generated TKE that is spent for the entrainment of the more buoyant free-atmospheric air versus being dissipated (Price et al. 1978; Part I).

A majority of previous studies (ZT77; TD81; D82; B84; BG94; P03; K05) directly account for the effects of

surface shear on entrainment. The near-surface shear production of TKE is parameterized in terms of the surface friction velocity u_*. The integral effect of the near-surface turbulence production is quantified through an effective velocity scale, which is a combination of u_* and the Deardorff (1970) convective velocity scale w_*. Other authors (like ML76) exclude the surface shear effects in the integral TKE budget considerations, assuming that the entire surface shear-generated TKE dissipates in the near-surface portion of the CBL and is therefore not available for entrainment. In Part I, it was found that the surface shear affects entrainment only in an indirect manner, through its influence on the mean mixed layer momentum. In the present part of the study, the effects of surface shear will be quantified more directly by testing the entrainment parameterizations that include the effects of surface layer shear.

In parameterizations that directly take the entrainment zone shear into account (ML76; ZT77; TD81; D82; B84; P03; SR04), the quantification of the TKE generated by entrainment zone shear is obtained from the integration of the shear production term of the TKE balance equation in the entrainment zone. The fraction of the integral shear-generated TKE spent for the entrainment in this case stands out clearly in the integral TKE budget equation, much like it does in the case of the buoyancy-generated TKE. However, unlike the latter case in which the entrainment fraction is generally agreed to be about 0.2 (Stull 1973; Fedorovich et al. 2004a; Part I), little direct experimental evidence exists to support the typically assumed value of 0.7 for the entrainment zone shear-generated TKE. As will be shown below (see section 4), the assumption regarding this fraction plays a particularly important role in the ability of entrainment equations to accurately predict the evolution of the CBL.

Another central issue regarding bulk model–based predictions of entrainment is the order (type) of bulk model used for representation of the CBL structure. The ZOM is the simplest representation of the CBL structure, and the ZOM-derived integral TKE budget (Fedorovich 1995) expresses integral shear and buoyancy production of TKE in a compact form that facilitates clear conceptual understanding of the processes contributing to the entrainment. However, some authors (e.g., Sullivan et al. 1998; vanZanten et al. 1999) suggest that at least a FOM representation of the CBL structure is necessary to capture essential features of the CBL related to entrainment. By accounting for the finiteness of the interfacial layer, the FOM also allows a more direct representation of the effects of Kelvin–Helmholtz-type instabilities in the entrainment zone of sheared CBLs. Such instabilities are associated with shear in the entrainment zone, and the existence of these instabilities appears to be dependent on a Richardson number in the entrainment zone (Kim et al. 2003; Sorbjan 2004; Part I). The exact definition of this Richardson number is dependent upon the author, but within the FOM approach, a concept of critical Richardson number, local to the entrainment zone, can be employed to reflect the balance between relative buoyancy and velocity changes with height at the top of a sheared CBL (ML76). Such a balance cannot be directly represented in the ZOM and, if it is an essential feature of entrainment, one might expect the FOM-based entrainment equations to more accurately reproduce the sheared CBL evolution.

In section 2, previously proposed bulk model parameterizations accounting for sheared convective entrainment are summarized, and derivations of the most commonly used parameterizations are outlined. Section 3 details the procedure used to evaluate the bulk model parameterizations against the LES cases described in Part I, and section 4 presents the results of those evaluations. Section 5 discusses the conclusions derived from the parameterization evaluations.

2. Background

The TKE balance equation forms the cornerstone of most entrainment parameterizations suggested to date. Derivation of the integral TKE balance equation for the CBL presents an opportunity to review the assumptions made along the way and to show in which aspects various entrainment parameterizations differ from one another. For those parameterizations whose underlying assumptions differ significantly from what we present below (i.e., use of a higher-order model or different mathematical formulation), we show only the resulting equation and refer to the original publication for details of the derivation.

a. Commonly used bulk model approaches

In the CBL bulk models, the entrainment equations are derived assuming a horizontally homogeneous, temporally evolving CBL flow in which the first- and second-order turbulence statistics, obtained by averaging over horizontal planes, represent ensemble-mean profiles of corresponding meteorological quantities. With these considerations in mind, one begins with the Reynolds-averaged Navier–Stokes (RANS) equations describing the CBL with horizontally averaged profiles of buoyancy $\overline{b} = g/\theta_0(\overline{\theta} - \theta_0)$ and horizontal velocity components $\overline{u}$ and $\overline{v}$ as related to vertical turbulent fluxes of buoyancy $B = (g/\theta_0)\overline{w'\theta'} = \overline{w'b'}$ and components of horizontal momentum, $\tau_x = -\overline{w'u'}$ and

$\tau_y = -\overline{w'v'}$ (Fedorovich 1995). In the above expressions, g is the gravitational acceleration, θ is potential temperature (to be inclusive of the presence of water vapor, θ could refer to virtual potential temperature), θ_0 is the reference value of θ (we use $\theta_0 = 300$ K), w is vertical velocity, overbars denote horizontal averages, and primes indicate deviations from horizontal averages. From this point forward, overbars will be omitted in the notation for the first-order moments (mean flow values) of meteorological variables.

Under the assumptions of horizontal homogeneity, the mean vertical velocity is zero, and the horizontal derivatives of all quantities are also zero. This implies that horizontal advection, as would occur in baroclinic conditions, is also zero. Therefore, one limitation of the bulk models, as described here, is that they do not account for differential temperature advection and vertical motion that may become important in baroclinic CBLs, as is discussed in SR04. With these assumptions, the mean velocity components u and v are related to their corresponding vertical kinematic turbulent fluxes τ_x and τ_y and the geostrophic wind components u_g and v_g through the equations describing the rate of change of velocity:

$$\frac{\partial u}{\partial t} = \frac{\partial \tau_x}{\partial z} + f(v - v_g), \tag{1}$$

$$\frac{\partial v}{\partial t} = \frac{\partial \tau_y}{\partial z} - f(u - u_g), \tag{2}$$

where f is the Coriolis parameter. If radiative fluxes and advection are also omitted, the rate of change of the mean buoyancy b is related only to the divergence of the vertical buoyancy flux:

$$\frac{\partial b}{\partial t} = -\frac{\partial B}{\partial z}. \tag{3}$$

The equation describing the TKE e changes in the horizontally homogeneous CBL is

$$\frac{\partial e}{\partial t} = \tau_x \frac{\partial u}{\partial z} + \tau_y \frac{\partial v}{\partial z} + B - \frac{\partial \Phi}{\partial z} - \varepsilon, \tag{4}$$

where $\Phi = (\overline{w'e'} - \rho_0^{-1}\overline{w'p'})$ is the vertical transport of TKE (ρ_0 is a reference density and p is pressure), and ε is the TKE dissipation rate.

To derive equations describing the CBL integral momentum, buoyancy, and TKE budgets (1) through (4) are vertically integrated over the depth of the CBL. To simplify these integrations, the overall CBL structure can be represented in a schematic form, as long as the schematic profiles capture the essential features of the CBL. In this section, we will review the development of the ZOM-based entrainment equations since they are the simplest and most commonly used. Figure 1 displays the ZOM representation of the CBL structure. At the CBL top ($z = z_i$) in the ZOM are zero-order discontinuities in buoyancy Δb and velocity components Δu and Δv. Above the CBL, the buoyancy changes at a linear rate of $\partial b/\partial z = N^2$, where N is the Brunt–Väisälä frequency. The velocity components also have a linear dependence on height in the free atmosphere: $\partial u/\partial z = \Gamma_u$, and $\partial v/\partial z = \Gamma_v$. In the baroclinic atmosphere, temperature advection can cause N, Γ_u, and Γ_v to vary with time, but the present study is focused on barotropic or equivalent barotropic conditions (Part I), so we take these quantities as constants.

The full set of ZOM equations for the horizontally homogeneous sheared CBL includes the following relationships (Fedorovich 1995):

$$\frac{d}{dt}\left(\frac{\Gamma_u}{2} z_i^2 - \Delta u z_i\right) = -\tau_{xs} + f\left(\frac{\Gamma_v}{2} z_i^2 - \Delta v z_i\right), \tag{5}$$

$$\frac{d}{dt}\left(\frac{\Gamma_v}{2} z_i^2 - \Delta v z_i\right) = -\tau_{ys} - f\left(\frac{\Gamma_u}{2} z_i^2 - \Delta u z_i\right), \tag{6}$$

$$\frac{d}{dt}\left(\frac{N^2 z_i^2}{2} - \Delta b z_i\right) = B_s, \tag{7}$$

$$\frac{d}{dt}\int_0^{z_i} e\, dz = u_m \tau_{xs} + v_m \tau_{ys} + \frac{1}{2}(\Delta u^2 + \Delta v^2) \times \frac{dz_i}{dt} + \frac{z_i}{2}\left(B_s - \Delta b \frac{dz_i}{dt}\right) - \Phi_i - \int_0^{z_i} \varepsilon\, dz, \tag{8}$$

where the various terms have been defined above and in Fig. 1. Equations (5) and (6) describe the integral budget of momentum, Eq. (7) describes the integral budget of buoyancy, and Eq. (8) is the integral TKE equation. Equations (5) through (8) do not form a closed set since the surface momentum fluxes $-\tau_{xs}$ and $-\tau_{ys}$, mixed layer velocity u_m and v_m, energy flux at the CBL top Φ_i, and the integrals of TKE e and dissipation ε are still unknown. The first two terms on the right-hand side of (8) represent the surface shear generation of TKE, the third term represents the entrainment zone shear production of TKE, and the fourth term represents the contribution of integral buoyancy flux to the TKE budget. The latter term consists of a positive part due to flux from the surface, B_s, and a negative part due to entrainment flux, $(-\Delta b\, dz_i/dt)$.

The derivation of the entrainment equation hinges

on the TKE equations, (8) or (4), with some authors (ZT77; TD81; D82) using (4) applied locally in the entrainment zone and others (ST76; B84; BG94) using the TKE equation integrated over the CBL depth (8). Although the methods of derivation and the parameterizations used are different, the resulting entrainment equations are essentially the same. In the present review, the integral approach is discussed.

Invoking a drag coefficient parameterization $C_D = u_*^2/(u_m^2 + v_m^2) = u_*^2/|\mathbf{u}_m|^2$, where $u_*^2 = (\tau_{xs}^2 + \tau_{ys}^2)^{1/2}$ is the surface friction velocity and $\mathbf{u}_m$ is the mixed layer velocity vector (B84; Garratt 1992), the surface shear production of TKE can be parameterized as $u_m\tau_{xs} + v_m\tau_{ys} = |\mathbf{u}_m|u_*^2 = C_D^{-1/2}u_*^3$. Noting the definition of the Deardorff (1970) convective velocity scale $w_* = (B_s z_i)^{1/3}$, the positive part of the buoyancy term can be written in terms of w_*. Also, under typical atmospheric conditions, the upward energy transport from the CBL top can be neglected (Stull 1976b; Fedorovich et al. 2004a). With these three changes, (8) becomes

$$\frac{d}{dt}\int_0^{z_i} e\,dz = C_D^{-1/2}u_*^3 + \frac{1}{2}(\Delta u^2 + \Delta v^2)\frac{dz_i}{dt} + \frac{1}{2}w_*^3 - \frac{1}{2}\Delta b z_i\frac{dz_i}{dt} - \int_0^{z_i}\varepsilon\,dz\,. \tag{9}$$

If one further assumes that the integral dissipation rate of TKE consists of the sum of the dissipation of the TKE generated by surface shear, entrainment zone shear, and surface buoyancy flux (a hypothesis that is difficult to test, yet it is at least implicitly made in all the entrainment parameterizations), the integral of dissipation can be split according to individual processes contributing to the TKE generation:

$$\frac{d}{dt}\int_0^{z_i} e\,dz = \left[C_D^{-1/2}u_*^3 - \int_0^{z_i}\varepsilon_{ss}\,dz\right] + \left[\frac{1}{2}(\Delta u^2 + \Delta v^2)\frac{dz_i}{dt} - \int_0^{z_i}\varepsilon_{es}\,dz\right] + \left[\frac{1}{2}w_*^3 - \int_0^{z_i}\varepsilon_B\,dz\right] - \frac{1}{2}\Delta b z_i\frac{dz_i}{dt}, \tag{10}$$

where ε_{ss}, ε_{es}, and ε_B are the dissipation rates of surface layer shear–, entrainment zone shear–, and buoyancy-generated TKE, respectively. The brackets associate each integral TKE production mechanism with its corresponding integral dissipation rate. Equation (10) shows that the TKE consumed by entrainment can come from any of the three production mechanisms, as long as that TKE is neither dissipated nor taken up by the reservoir of TKE in the CBL.

The integrals of TKE and dissipation can be simplified by selecting appropriate length and velocity scales in the CBL, and the mathematical form of (10), as well as physical considerations, suggest the best approach would be to choose the same scaling parameter for the production and dissipation of each type of TKE. For the buoyancy-generated TKE, the obvious choice is w_*^2. Following Zilitinkevich (1991) [see also Eq. (6) of Fedorovich et al. (2004a)], we can choose z_i as the length scale and write

$$\varepsilon_B = \frac{w_*^3}{z_i}\varphi_{\varepsilon B}(\zeta), \tag{11}$$

where $\zeta = z/z_i$ and $\varphi_{\varepsilon B}$ is a dimensionless function of dimensionless height. When integrated over the depth of the CBL, (11) becomes

$$\int_0^{z_i}\varepsilon_B\,dz = C_{\varepsilon B}w_*^3, \tag{12}$$

where $C_{\varepsilon B}$ is a universal constant, which has been shown (Zilitinkevich 1991; Fedorovich et al. 2004a) to have a value of about 0.4 in the shear-free CBL. Essentially, (12) implies that a constant fraction of the surface buoyancy–produced TKE is dissipated. For the surface shear-generated TKE, the natural scale is u_*^2, and choosing z_i as the length scale, we find that

$$\int_0^{z_i}\varepsilon_{ss}\,dz \propto u_*^3. \tag{13}$$

For the entrainment zone shear–generated TKE, there is no obvious velocity scale aside from the combination of velocity jumps and entrainment rate associated with the entrainment zone shear production of TKE, so it is most straightforward to assume that a constant fraction of the shear-generated TKE in the entrainment zone is dissipated:

$$\int_0^{z_i}\varepsilon_{es}\,dz \propto (\Delta u^2 + \Delta v^2)\frac{dz_i}{dt}. \tag{14}$$

This is effectively the same as what is done in (12) for the surface shear– and buoyancy-generated TKE. Because the production and dissipation are scaled the same way and are therefore linearly related, we can simplify (10) and, for each production mechanism, absorb the fraction of dissipated TKE and associated constants into new constants of proportionality. The integral TKE budget then becomes

$$2\frac{d}{dt}\int_0^{z_i} e\,dz = C_s u_*^3 + C_P(\Delta u^2 + \Delta v^2)\frac{dz_i}{dt} + C_1 w_*^3 - \Delta b z_i \frac{dz_i}{dt}, \quad (15)$$

where C_S is a constant associated with the surface shear generation of TKE (the fraction of surface shear-generated TKE available for entrainment is $C_s' = C_s C_D^{1/2}$), C_p is the fraction of entrainment zone shear–generated TKE available for entrainment, and C_1 represents the same for the buoyancy-generated TKE.

The left-hand side of (15) requires careful treatment. Typically, the integral TKE in the CBL is scaled by the square of a characteristic velocity scale multiplied by a length scale. For the shear-free CBL, the scaling parameters are w_* and z_i (Zilitinkevich 1991), and the left-hand side of (15) would become

$$C'_T\frac{d}{dt}(w_*^2 z_i) = C'_T\frac{d}{dt}(B_s^{2/3} z_i^{5/3}) = C''_T w_*^2\frac{dz_i}{dt}, \quad (16)$$

where C'_T is the scaling constant associated with the rate of change of integral TKE (the temporal term) and the constants associated with the differentiation are absorbed into the constant C''_T. According to Zilitinkevich (1991), $C''_T = 1.7$.

If shear-generated TKE is also present, then additional scalings have to be introduced. The friction velocity u_* may be added as a scaling parameter associated with surface layer shear–generated TKE, and perhaps $(\Delta u^2 + \Delta v^2)\,dz_i/dt$ would be an appropriate quantity for determination of the velocity scale associated with the entrainment zone shear–generated TKE. To be consistent with the mathematical methodology and physical considerations regarding the temporal term, the choice of scaling parameters should be made before the time derivative on left-hand side of (15) is evaluated. Let us choose w_*, u_*, and $[(\Delta u^2 + \Delta v^2)\,dz_i/dt]^{1/3}$ as the velocity scales, and let A_1', A_2', and A_3' be the respective constants of proportionality [resulting from integration of dimensionless functions of normalized height z/z_i; see Fedorovich et al. (2004a)]. Since all three scalings include time-dependent variables, the left-hand side of (15) becomes much more complicated:

$$2\frac{d}{dt}\int_0^{z_i} e\,dz = \frac{d}{dt}\left\langle \left\{ A_1' w_*^2 + A_2' u_*^2 + A_3'\left[(\Delta u^2 + \Delta v^2)\frac{dz_i}{dt}\right]^{2/3}\right\} z_i \right\rangle. \quad (17)$$

In particular, the resulting system of differential equations becomes second order in time.

Most authors of the previously suggested entrainment parameterizations short-circuit this whole process and simply write down the left-hand side of (15) in terms of another velocity scale σ_w, which is commonly assumed to be a combination of w_* and u_* scales (see below). However, such an approach may not be consistent with the physical processes associated with the temporal term; this issue will be saved for future research. Using the simplified scaling, the TKE budget equation becomes

$$C_T\sigma_w^2\frac{dz_i}{dt} = C_s u_*^3 + C_P(\Delta u^2 + \Delta v^2)\frac{dz_i}{dt} + C_1 w_*^3 - \Delta b z_i\frac{dz_i}{dt}, \quad (18)$$

where C''_T has been replaced by C_T, which, generally speaking, may vary in time, if the simplified scaling is assumed. Solving for dz_i/dt yields

$$\frac{dz_i}{dt} = \frac{C_1 w_*^3 + C_s u_*^3}{\Delta b z_i + C_T\sigma_w^2 - C_P(\Delta u^2 + \Delta v^2)}. \quad (19)$$

If we define $A = C_S/C_1$, the numerator can be written in terms of another combined velocity scale, w_m, introduced as $w_m^\eta = w_*^\eta + A u_*^\eta$, $\eta = 3$ (note that some authors use $\eta = 2$ in this scaling, see Table 1). Additionally, most authors assume $\sigma_w = w_m$ (although they are not necessarily the same), so the entrainment equation becomes

$$\frac{dz_i}{dt} = \frac{C_1 w_m^3}{\Delta b z_i + C_T w_m^2 - C_P(\Delta u^2 + \Delta v^2)}. \quad (20)$$

An expression for the ZOM entrainment flux ratio $-B_{i0}/B_s = \Delta b\,dz_i/dt$ is obtained through multiplying (20) by $\Delta b/B_s$:

$$\frac{\Delta b\,dz_i/dt}{B_s} = \frac{w_m^3}{w_*^3}C_1\Big/\left[1 + C_T\frac{w_m^2}{\Delta b z_i} - C_P\frac{(\Delta u^2 + \Delta v^2)}{\Delta b z_i}\right]. \quad (21)$$

TABLE 1. Values of constants in entrainment equations.

Author	A	η	C_1	C_T	C_P
Tennekes (1973)	12.5	3	0.2	0	0
Zeman and Tennekes (1977)	4.6	2	$0.5 - 0.024\frac{Nz_i}{w_m}$	3.55	$0.024\frac{Nz_i}{w_m}$
Tennekes and Driedonks (1981)	4	2	$0.6 - 0.03\frac{Nz_i}{w_m}$	4.3	0.7
Driedonks (1982)	25	3	0.2	0	0
Boers et al. (1984)	23	3	0.32	0.75	1
Batchvarova and Gryning (1991, 1994)	12.5	3	0.2	0	0
Pino et al. (2003)	8	3	0.2	4	0.7
Present study	0	3	0.2	0	0.4

We can further introduce the following Richardson numbers, which represent different buoyancy contributions to the TKE budget:

$$\mathrm{Ri}_t = \frac{\Delta b z_i}{w_m^2}, \quad \mathrm{Ri}_{\Delta b} = \frac{\Delta b z_i}{w_*^2}, \quad \mathrm{Ri}_{\mathrm{GS}} = \frac{\Delta b z_i}{(\Delta u^2 + \Delta v^2)},$$

$$\mathrm{Ri}_u = \frac{\Delta b z_i}{u_*^2}, \tag{22}$$

where Ri_t is associated with the temporal term and includes effects of surface shear, $\mathrm{Ri}_{\Delta b}$ is the same, except it excludes shear effects, $\mathrm{Ri}_{\mathrm{GS}}$ is the Richardson number associated with the entrainment zone shear, and Ri_u is associated with the surface layer shear. Substituting Ri_t and $\mathrm{Ri}_{\mathrm{GS}}$ into (20), we have

$$\frac{\Delta b\, dz_i/dt}{B_s} = \frac{w_m^3}{w_*^3} \frac{C_1}{[1 + C_T \mathrm{Ri}_t^{-1} - C_P \mathrm{Ri}_{\mathrm{GS}}^{-1}]}. \tag{23}$$

This is the basic form of the ZOM entrainment parameterization used by ZT77, TD81, D82, B84, and P03. The main differences among their entrainment equations lie in the values of the constants used. Table 1 lists the values of these constants for each entrainment equation. In a study of storm-induced mixed layer deepening in the ocean, Price et al. (1978) found $C_P = 0.7$, the value most commonly used in bulk parameterizations of entrainment. Note that the right-hand side of (23), in the shear-free case, reduces to the constant C_1. The most commonly used value for C_1 is 0.2, and the constancy of this value has been shown by Fedorovich et al. (2004a) over the typical range of atmospheric stratification considered in the present study, although Sorbjan (1996a,b) found that it can vary when the buoyancy jump Δb becomes very large or very small, outside the range of values encountered in the present study.

One potential problem is immediately seen by examining (21) or (23). If the shear becomes strong enough at the CBL top, the term involving $\Delta u^2 + \Delta v^2$ can exactly cancel the other terms, and the denominator becomes equal to zero. As this condition is approached, the predicted ZOM entrainment flux ratio increases to infinity, which is not realistic unless the surface buoyancy flux B_s approaches zero. If the shear further increases, the predicted ratio becomes negative, and this is also unrealistic. Such behavior of (23) is apparently a result of the insufficiency of the physical hypotheses underlying the problem or a consequence of some physical mechanisms unaccounted for in (22) that would cause the terms in the denominator of (23) to cancel each other. The additional temporal terms incorporated in (17) but dropped in (23) suggest that the nonstationarity of the TKE budget could be one of these missing physical mechanisms.

b. Other ZOM parameterizations

Some suggested entrainment parameterizations based on the ZOM approach differ from (23) only by the values of the constants A, η, C_1, C_T, and C_P. Others, however, employ different hypotheses regarding the dissipation of TKE in the entrainment zone, the effects of surface shear, entrainment zone shear, and the manner in which entrainment zone variables such as potential temperature jump are affecting the entrainment.

The parameterization of Tennekes (T73), which accounts only for the effects of surface shear on the entrainment, through the use of u_* in the velocity scaling, is essentially a truncated form of (23):

$$-\frac{B_{i0}}{B_s} = C_1\left(1 + A\frac{u_*^3}{w_*^3}\right) = C_1\frac{w_m^3}{w_*^3}. \tag{24}$$

Moeng and Sullivan (1994) found (24) to be a good representation of the characteristic velocity scale within sheared CBLs, and Driedonks (D82) found it to match some atmospheric datasets more closely than (23).

Stull (ST76) employed a set of arbitrary scaling assumptions regarding the mechanical generation of TKE at the inversion base. He assumed that τ_{xs} scaled by $\Delta u\ dz_i/dt$, but he also parameterized velocity shear in the entrainment zone as $\partial u/\partial z \sim \Delta u^2/(\delta_s\ dz_i/dt)$, where δ_s is the difference between the buoyancy flux zero crossing height and z_i in the ZOM. As a result of these assumptions, the problems associated with the denominator of (23) going to zero were circumvented:

$$-\frac{B_{i0}}{B_s} = A_1 + A_2\frac{u_*^2|u_m|}{B_s\delta_s} + A_3\frac{\Delta u^3}{B_s\delta_s}. \tag{25}$$

Best fits of this expression with atmospheric data presented in Stull (1976c) provide: $A_1 = C_1 = 0.1 \pm 0.05$, $A_2 = 0.05 \pm 0.025$, and $A_3 = 0.001 \pm 0.0005$. The entrainment zone shear term (the third term on the right-hand side) is somewhat problematic to interpret because Δu^3 can have either a positive or negative sign, depending on the orientation of the coordinate system. As written, (25) lacks Galilean invariance because it would predict opposite effects of shear on entrainment if the coordinate system is rotated 180° about the z axis. For the current study, the Δu^3 term will be interpreted as $|\Delta u^3|$.

Zeman and Tennekes (ZT77) developed their entrainment parameterization using a local TKE balance equation at the top of the CBL. The surface shear effects were included through the modified velocity scaling $e \approx w_m^2 = w_*^2 + 4.6u_*^2$, with the constant $A = 4.6$ determined from the water tank data of Kato and Phillips (1969). They also employed local, N-dependent scalings for the dissipation of both buoyancy- and shear-produced TKE in the entrainment zone (the same scaling for the dissipation of buoyancy-generated TKE is used in TD81). Conzemius and Fedorovich (2004) evaluated the ZT77 parameterization without the entrainment zone shear term, but in the present study we wish to evaluate the original ZT77 dissipation hypothesis regarding entrainment zone shear–generated TKE.

Batchvarova and Gryning (BG94) used a somewhat different approach toward derivation of the entrainment equation that involved the elimination of $\Delta\theta$, a dependent variable, from the entrainment equation by substituting a diagnostic equation that relates $\Delta\theta$ to the surface friction velocity, heat flux (both of which can be calculated from measured near-surface quantities), and CBL depth. Because they did not directly consider entrainment zone shear and because they eliminated $\Delta\theta$, their entrainment parameterization can be applied without evaluating any entrainment zone parameters, which adds utility to the parameterization when it is used with atmospheric data since entrainment zone parameters are often difficult or expensive to measure. The BG94 formula is

$$-\frac{B_{i0}}{B_s} = \frac{X_{\rm BG}(1 + X_{\rm BG})}{1 + X_{\rm BG} + Y_{\rm BG}(1 + 2X_{\rm BG})}, \tag{26}$$

where $X_{\rm BG} = w_m^3/w_*^3 = C_1(1 + Au_*^3/w_*^3)$, and $Y_{\rm BG} = B_{\rm BG}u_*^2/(N^2z_i^2)$ with $B_{\rm BG} = 8$.

c. Higher-order parameterizations

For sheared CBLs, the interface between the mixed layer and the free atmosphere should be expected to be more diffuse than in the shear-free case because of the broadening spectrum of contributing instabilities of various types, primarily Kelvin–Helmholtz instabilities (Kim et al. 2003). Therefore, an entrainment zone of a relatively large depth may be an essential feature of the sheared CBL and may need to be included in the schematic representation of the CBL structure. ML76, SR04, and K05 suggested entrainment parameterizations based on the higher-order CBL bulk models, the simplest of which is the FOM (Betts 1974). The FOM equations for the entraining CBL are considerably more complex than the ZOM equations, and some of the terms in those equations are difficult to interpret physically, so most authors prefer to make some assumptions that allow simplification of the equations.

Mahrt and Lenschow (ML76) assumed the entrainment zone thickness Δz to be much smaller than the CBL depth z_i, allowing numerous terms in the FOM-based equations to be neglected. In particular, terms of order Δz and higher were neglected in the momentum and buoyancy balance equations (which then acquire the same form as their ZOM counterparts), and terms of the order of Δz^2 and higher were neglected in the TKE equation. Also, if Δz is small relative to z_i, the parameterization $\overline{w'\phi'}_i = -\Delta\phi(dz_i/dt)$, which is an exact expression in the ZOM, can be used to approximate the fluxes at the CBL top in the FOM. The ML76 entrainment equation, written in a form consistent with (23), is

$$\frac{-B_i}{B_s} = \frac{\Delta b_1\ dz_i/dt}{B_s} = \frac{\left[1 + 2C_0 - 2C_\varepsilon\left(1 + \dfrac{\Delta z}{2z_i}\right)\right]}{\left(1 + \dfrac{\Delta z}{z_i}\right) - \dfrac{\Delta u_1^2 + \Delta v_1^2}{\Delta b_1 z_i}}, \tag{27}$$

where C_0 is the constant specifying the loss of TKE due to transport out of the CBL by gravity waves, and Δb_1, Δu_1, and Δv_1 are the FOM buoyancy and velocity changes at the CBL top. These FOM parameters are

designated with the subscript "1" because they are not exactly the same as their ZOM counterparts. Given the results of Stull (1976b), Fedorovich et al. (2004a), and Part I, for the present study we have assumed $C_0 = 0$ and $C_\varepsilon = 0.4$.

K05 suggested another FOM-based entrainment parameterization for sheared CBLs. Like ML76, they made some assumptions to simplify their FOM-based equations. Specifically, they approximated the buoyancy flux and momentum flux profiles as linear in the entrainment zone (in the full equations they are represented by quadratic terms), and they also took $d\Delta z/dt \simeq 0$. The resulting parameterization reads:

$$\frac{-B_{i1}}{B_s} = T_{\rm num} \Bigg/ \left(1 - \frac{[0.5(\Delta u_1 + \Delta \upsilon_1)]^2}{2(g/\theta_0)(\Delta\theta_1 - \Gamma_\theta \Delta z_K/2)(z_i + \Delta z_K)} A_{3K}\right), \tag{28}$$

where

$$T_{\rm num} = A_{1K}\frac{1}{1 + \Delta z_K/z_i} + A_{2K}\frac{u_*^3}{w_*^3} + A_{3K}\frac{1}{w_*^3}\frac{\Delta z_K}{(4z_i + 2\Delta z_K)}\left\{0.5u_*^2(\Delta u_1 + \Delta \upsilon_1) + \frac{\overline{w'\theta_s'}}{\Delta\theta_1 - \Gamma_\theta \Delta z_K/2}[0.5(\Delta u_1 + \Delta \upsilon_1)]^2\right\}. \tag{29}$$

In the above expressions, the constants of proportionality are $A_{1K} = 0.2$, $A_{2K} = 0.26$, and $A_{3K} = 1.44$, and the independent parameter Γ_θ is the linear change of potential temperature with respect to height above the CBL. One possible shortcoming of this formula is the representation of the velocity change across the entrainment zone by the expression $0.5(\Delta u_1 + \Delta \upsilon_1)$ rather than, for instance, $(\Delta u_1^2 + \Delta \upsilon_1^2)^{1/2}$. The former expression provides a physically confusing entrainment formula if the signs of the velocity components are opposite, but their moduli are large.

The entrainment zone thickness Δz_K in K05 is parameterized by the diagnostic formula

$$\Delta z_K = z_i(1.12{\rm Ri}_k^{-1} + 0.08), \quad \text{where}$$
$$ {\rm Ri}_k = \frac{\Delta b_1 z_i}{w_*^2 + 4u_*^2 + 0.1(\Delta u_1^2 + \Delta \upsilon_1^2)}. \tag{30}$$

We have made a distinction between the entrainment zone thickness Δz_K adopted in K05 and the FOM entrainment zone thickness $\Delta z = z_{iu} - z_i$ (see Fig. 1 for definitions of z_{iu} and z_i) because of the different specifications of these quantities. However, to evaluate (28), we will use Δz because determination of the jumps Δb_1, Δu_1, and $\Delta \upsilon_1$ requires knowledge of Δz. Otherwise, Δz_K in (30) needs to be determined iteratively from atmospheric or simulation data.

Recently, Sorbjan (SR04) developed a parameterization specifically designed to predict the heat flux at the sheared CBL top. This parameterization takes into account a bulk Richardson number in the entrainment zone and therefore implies a finite entrainment zone thickness. The SR04 parameterization is

$$B_{i1} = c_H w_*^2 N_i \frac{(1 + c_{2S}/{\rm Ri}_\delta)}{(1 + 1/{\rm Ri}_\delta)^{1/2}}, \tag{31}$$

with $c_H = -0.0075$ and $c_{2S} = 1.5$. In (31), $N_i = (\delta b/\delta z_i)^{1/2}$ is the Brunt–Väisälä frequency within the interfacial layer, and the interfacial Richardson number ${\rm Ri}_\delta$ is defined as ${\rm Ri}_\delta = (\delta b \delta z_i)/(\delta u^2 + \delta v^2)$, where the velocity and buoyancy jumps are interpreted as their changes across the entire entrainment zone $\delta z_i = z_{iu} - z_{il}$ (see Fig. 1). The parameterization asymptotically approaches either an expression describing a purely shear-driven CBL or one describing a purely buoyancy-driven CBL, depending on the relative contributions of shear and buoyancy to the evolution of the CBL. It only takes the entrainment zone shear into account and neglects surface shear.

3. Evaluation of entrainment equations and parameterizations

a. Large-eddy simulations

The output of a total of 24 LES runs, described in Part I, was used to test the parameterizations against conditions of varying shear, outer stratification, and surface buoyancy flux. Main features of the conducted simulations, the parameter space for the simulated CBLs, and the statistics calculated from LES are described in detail in Part I. The simulations cover outer temperature gradient values of $\partial\theta/\partial z = 0.001$ K m^{-1}, and $\partial\theta/\partial z = 0.003$ K m^{-1}, and $\partial\theta/\partial z = 0.01$ K m^{-1}

($N = 0.006\ \mathrm{s}^{-1}$, $N = 0.01\ \mathrm{s}^{-1}$, and $N = 0.018\ \mathrm{s}^{-1}$, respectively) as well as surface kinematic temperature flux values of $Q_s = 0.03\ \mathrm{K\ m\ s}^{-1}$, $Q_s = 0.01\ \mathrm{K\ m\ s}^{-1}$, and $Q_s = 0.3\ \mathrm{K\ m\ s}^{-1}$ (buoyancy flux of $B_s = 0.001\ \mathrm{m}^2\ \mathrm{s}^{-3}$, $B_s = 0.003\ \mathrm{m}^2\ \mathrm{s}^{-3}$, and $B_s = 0.01\ \mathrm{m}^2\ \mathrm{s}^{-3}$, respectively). The simulations are divided among three categories of shear: a simulation set with background conditions of no mean wind or wind shear (NS); a simulation set with a height-constant geostrophic wind of 20 $\mathrm{m\ s}^{-1}$ (GC); and a simulation set in which the geostrophic wind speed varies as a function of height throughout the domain, ranging from 0 $\mathrm{m\ s}^{-1}$ at the surface to 20 $\mathrm{m\ s}^{-1}$ at the top of the simulation domain (GS). The NS, GS, and GC designations will be used for the remainder of the text to refer to the type of shear encountered by the growing CBL in each particular simulation. The GS cases were primarily designed to investigate the effects of shear at the CBL top on the entrainment, and the GC cases were designed for investigation of the effects of surface layer shear.

b. Method of evaluation

There are several ways to evaluate the entrainment parameterizations discussed in section 2 against the LES data from Part I. The first is to evaluate (23) through (28) and (31), retrieving the parameters of entrainment from LES in a consistent manner with their definitions in the respective models of the CBL. Such evaluations yield model-predicted entrainment flux ratios, as a function of time, for the parameters of entrainment (CBL depth, buoyancy and velocity changes in the entrainment zone, surface friction velocity) as they appear at that time in LES. Alternatively, the full set of equations describing the CBL evolution can be integrated for each of the derived parameterizations, and their predictions of $z_i(t)$ can be compared against LES. However, not all parameterizations discussed above are accompanied by corresponding momentum and buoyancy balance equations for the CBL, which would be necessary to include them in such a test.

Because we solved for dz_i/dt on the way to deriving (23), the latter expression should capture the behavior of the different parameterizations just as well as if they were used to predict $z_i(t)$, given initial values of z_i, Δu, Δv, and $\Delta\theta$ retrieved from LES. Based on this consideration, the entrainment flux ratio predicted by the respective parameterizations, as discussed above, will serve as the benchmark for comparing the bulk model predictions with LES.

c. Retrieval of parameters of entrainment from LES

To have sense, the equations and parameterizations must be interpreted fully within the model framework in which they were developed (Fedorovich et al. 2004a). If the parameterization is developed from the ZOM, then the integral parameters of entrainment input to the parameterization must be interpreted according to the ZOM, as shown in Fig. 1; the same is true for the FOM. There must also be consistency between the ZOM, FOM, and LES regarding the notion of the CBL depth z_i (Fedorovich et al. 2004a) as well as with respect to the interpretation of the CBL buoyancy (D82) and momentum distributions.

We interpret the CBL depth z_i as the minimum in the buoyancy flux profile. This is a definition of z_i that is common to the ZOM, FOM, and LES. Another popular CBL depth definition, from the maximum potential temperature gradient, loses sense in the FOM, where temperature (buoyancy) gradient is constant over the entire entrainment zone. Additional reasons for using the heat flux minimum height as the CBL depth scale are discussed in Fedorovich et al. (2004a).

In the ZOM, the buoyancy jump Δb is interpreted as the difference between the free-atmosphere buoyancy value, extrapolated to z_i, minus the mixed layer buoyancy, which is the average buoyancy value below z_i. However, rather than using $b(z_{il})$ as a representation of the mixed layer buoyancy as in Fedorovich et al. (2004a), we calculate from LES data the vertical average of b below z_i (the two actually turn out to be very close to one another). Additionally, above z_i, we integrate the buoyancy difference between the LES buoyancy profile versus the free-atmospheric profile and add this integral difference to the integral mixed layer buoyancy, before dividing by z_i, to obtain the mixed layer buoyancy value, b_m (see Fig. 2a):

$$b_m = \frac{1}{z_i}\left[\int_0^{z_i} b_{\mathrm{LES}}\, dz + \int_{z_i}^{\infty} (b_{\mathrm{LES}} - b_{\mathrm{init}})\, dz\right], \tag{32}$$

where $b_{\mathrm{init}}(z)$ is the initial ($t = 0$) LES profile in the free atmosphere, which is constant with time, and b_{LES} is the LES horizontally averaged LES buoyancy profile at time t. The buoyancy jump at the interface is then $\Delta b = b_{\mathrm{init}}(z_i) - b_m$. Examination of the LES data has shown that most of this integral buoyancy difference above z_i is associated with the diffuse nature of the entrainment interface. Performing the operation inside the brackets of (32) essentially amounts to putting the excess buoyancy just below z_i back just above z_i. The same procedure is used to determine Δu and Δv. Although this method may appear to artificially force the LES profiles to be ZOM-like when the interfacial layer might truly be diffuse in a mean sense, the method is the most consistent with the conceptual framework of the ZOM,

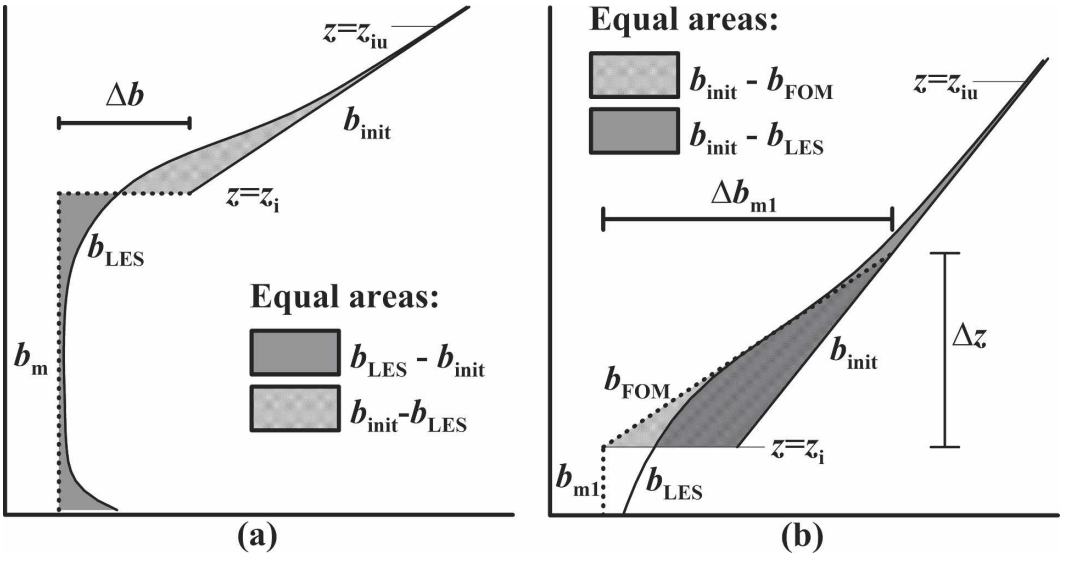

FIG. 2. Determination of the (a) ZOM and (b) FOM parameters of entrainment from LES data. To determine the mixed layer buoyancy b_m, the hatched area in (a) is subtracted from the integrated buoyancy between $z = 0$ and $z = z_i$. The shaded area is equal to the hatched area. In (b), the view is focused on the entrainment zone, and Δb_1 is constrained to the value for which the shaded and hatched areas are equal (b_{FOM} is a linear function of z), and b_{m1} is defined as the average LES buoyancy between $z = 0$ and $z = z_i$.

and it extracts ZOM parameters of entrainment from LES in a manner that ensures conservation of integral buoyancy and momentum between the LES and ZOM profiles. D82 has also discussed the need for conservation of integral buoyancy.

The same integral buoyancy and momentum conservation principles are used to retrieve FOM parameters of entrainment from LES (see Fig. 2b). First, the CBL depth z_i is determined from the LES profile. The FOM mixed layer buoyancy b_{m1} is then determined by averaging the LES buoyancy below z_i. Above z_i, the integral buoyancy difference between LES and the free-atmospheric profile is calculated in the same manner as described above, but, instead of adding it to the integral mixed layer buoyancy, the integral difference is used as a constraint to determine the FOM interfacial layer thickness Δz:

$$\int_{z_i}^{\infty} (b_{\mathrm{LES}} - b_{\mathrm{init}})\, dz = \int_{z_i}^{z_i+\Delta z} (b_{\mathrm{FOM}} - b_{\mathrm{init}})\, dz, \qquad (33)$$

assuming a linear profile of b_{FOM} in the entrainment zone as defined in the FOM (see Fig. 2b). Using this constraint, the entrainment zone depth is found to be

$$\Delta z = \frac{2\int_{z_i}^{\infty} (b_{\mathrm{init}} - b_{\mathrm{LES}})\, dz}{b_{\mathrm{init}}(z_i) - b_{m1}}. \qquad (34)$$

Analysis of LES output shows that Δz retrievals from this method are very close to what they would be if Δz were defined as the difference between the upper interface of the entrainment zone z_{iu} and the CBL top z_i.

d. *Differing interpretations of buoyancy and velocity jumps*

Occasionally, it was clear that the authors of the discussed entrainment parameterizations interpreted the buoyancy and velocity jumps across the entrainment zone rather differently when retrieving them from LES or atmospheric data. Since the authors often selected the constants such as A, C_1, C_T, and C_P based on tests of their parameterizations against LES or atmospheric data, it is probably best to test those parameterizations in a manner consistent with the way they were tested by the original authors. To the extent possible, we interpret the buoyancy and velocity jumps the way they were interpreted by the original authors. In particular, P03 interpreted the jumps retrieving buoyancy and velocity at the level where the horizontally averaged potential temperature gradient first became equal to or greater than the free-atmospheric potential temperature gradient and subtracting, from those values, the mixed layer values, which were taken at the 11th LES grid level (D. Pino 2003, personal communication; Fedorovich et al. 2004c). In most cases, the original author's precise definitions of the jumps was not known, so the procedure outlined above served as the default,

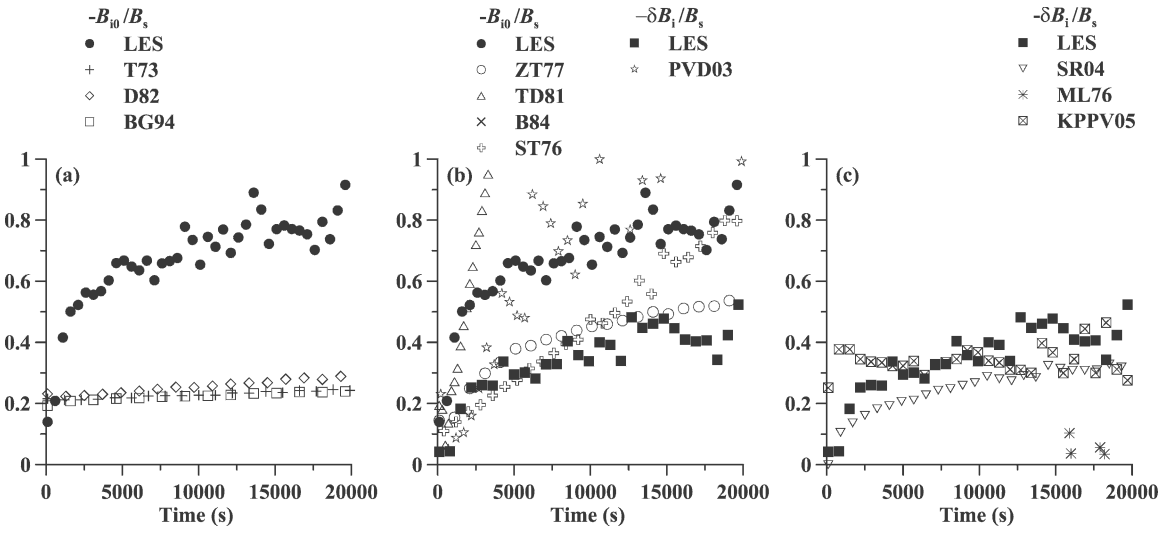

FIG. 3. Entrainment flux ratio predicted for the GS case with $\partial\theta/\partial z = 0.003$ K m^{-1} and $Q_s = 0.03$ K m s^{-1} by LES and the entrainment parameterizations classified according to the following categories: (a) ZOM, surface shear only; (b) ZOM, surface and entrainment zone shear; (c) FOM and other higher-order closures. The outputs from LES and parameterizations are labeled with the following symbols: LES $-B_{i0}/B_s$ (solid dots); LES $-\delta B_i/B_s$ (solid squares); T73 (crosses); D82 (open diamonds); BG94 (open squares); ZT77 (open circles); TD81 (open triangles); B84 (×); ST76 (open crosses); P03 (open stars); SR04 (inverted triangles); ML76 (asterisks); and K05 (hatched open squares).

and therefore, our definitions of the jumps may occasionally be different from those of the original authors.

4. Results of testing

The results of our simulations (see Part I) show that the most fruitful comparisons between the simulations and the parameterizations can be made by focusing on a subset of the simulated cases. For reasons explained in Part I, we focus here on the GS and GC cases with the following values of free-atmosphere stratification and surface heat flux:

(subsection *a*) $\partial\theta/\partial z = 0.003$ K m^{-1} and $Q_s = 0.03$ K m s^{-1};
(subsection *b*) $\partial\theta/\partial z = 0.01$ K m^{-1} and $Q_s = 0.1$ K m s^{-1};
(subsection *c*) $\partial\theta/\partial z = 0.01$ K m^{-1} and $Q_s = 0.3$ K m s^{-1}.

a. $\partial\theta/\partial z = 0.003$ K m^{-1} and $Q_s = 0.03$ K m s^{-1}

1) GS CASE

Figure 3 shows the comparisons between the LES-predicted entrainment flux ratios A_R (see Part I) and the parameterization predictions of entrainment flux ratios. The parameterizations are grouped according to the following classes: (i) ZOM-based parameterizations including the effects of surface shear but not entrainment zone shear; (ii) ZOM parameterizations including both surface and entrainment zone shear; and (iii) FOM parameterizations. Some of the parameterizations predict the LES ratio $\delta B_i/B_s$ while others predict $-B_{i0}/B_s = A_R$, which is the ZOM representation of the heat flux at the top of the CBL (see Part I). Since these two ratios are not the same (see Fig. 1), they are both presented from the LES data for comparison with the parameterization results. The same groupings (i), (ii), and (iii) will be used for the remaining figures in this section.

In Fig. 3a, the parameterized entrainment flux ratio $-B_{i0}/B_s$ is consistently less than $-B_{i0}/B_s$ derived from LES. In fact, the parameterized $-B_{i0}/B_s$ does not depart significantly from the commonly accepted shear-free value of 0.2, and for much of the simulation, the parameterized $-B_{i0}/B_s$ is also less than the $-\delta B_i/B_s$ ratio from LES. Since these ZOM-based parameterizations include only the effects of surface shear on entrainment, they are unable to model the effects of the entrainment zone shear that are dominant in the GS cases.

The ZOM parameterizations that take into effect the entrainment zone shear can, under certain conditions, model the entrainment flux ratio more accurately (see Fig. 3b). However, in many cases, these parameterizations overpredict the entrainment flux ratio. In particular, the TD81 parameterization predicts a rapidly increasing ratio as the entrainment zone shear increases during the simulation, and the B84 parameterization

does not even predict a realistic $-B_{i0}/B_s$ (its predicted values do not fall within the range shown in Fig. 3b); its denominator becomes very small or jumps around either side of zero, resulting in wild fluctuations of the parameterized $-B_{i0}/B_s$. Although the TD81 parameterization more accurately predicts the entrainment flux ratio, the denominators of B84 and TD81 differ only by the values of the constants C_T and C_P, so the inherent weakness of all parameterizations of the form (23) can be seen. B84 has a smaller C_T, resulting in less parameterized TKE take-up by the reservoir within the CBL interior, and $C_P = 1$, so all of the TKE generated by entrainment zone shear is assumed to be used for entrainment. It appears that this fraction should actually be much smaller (see Part I). The P03 parameterization is also of the form of (23), but it was used with its own specific criteria for the velocity and buoyancy jumps at the CBL top (see above), and with those criteria, the P03 parameterization seems to agree reasonably well with $-B_{i0}/B_s$ from LES. However, the P03 parameterization is tuned to predict $\delta B_i/B_s$, which, as derived from LES, is much less in Fig. 3b. The P03 predictions show considerable scatter during the simulation, symptomatic of the denominator becoming rather small and the output of the parameterization becoming very sensitive to small changes in Δu, Δv, and Δb. The constant C_P in P03 is smaller and C_T is larger than in B84, so its predictions of the entrainment flux ratio are closer to the LES-derived ratios. The ZT77 parameterization has the same form as B84 and TD81, but the assumptions regarding the dissipation of entrainment zone shear-produced TKE are different, and those assumptions appear to work better for this particular GS case. The ZT77 parameterization of $-B_{i0}/B_s$ seems to fall between the two LES-derived entrainment flux ratios, and the time-dependent behavior of the ZT77 parameterization mimics that of the LES $-B_{i0}/B_s$. The ST76-parameterized $-B_{i0}/B_s$ also compares favorably with the LES values overall, but its time dependency differs from LES.

With the exception of the ML76 parameterization, the higher-order model parameterizations show improved predictions of the entrainment flux ratio compared to the ZOM-based parameterizations (see Fig. 3c). The FOM-based parameterizations of ML76 (27) and K05 (28) include the entrainment zone shear term in the denominator, with the accompanying, potentially negative consequences. The integral method used to derive these FOM parameterizations is essentially the same as that used in the ZOM, so, although the order of the model is higher, the parameterizations appear subject to the effects of similarly formulated mathematical or physical assumptions as those inherent in (23). However, the K05 parameterization predicts entrainment flux ratios that match the LES ones rather well. It must be noted that the dissipated fraction of entrainment zone shear-generated TKE assumed by K05 is approximately the same as used in TD81 and P03, yet the K05 parameterization provides better agreement with the LES entrainment flux ratio $-\delta B_i/B_s$ than either of the TD81 or P03 parameterizations. This again suggests that the entrainment zone thickness Δz is an important parameter to include in the entrainment equations for the sheared CBL. The ML76 model employs a dissipation parameterization that results in the dissipation of TKE becoming decoupled from its production, and this appears to be the primary reason behind its relatively poor predictions of $-\delta B_i/B_s$.

The SR04 parameterization predictions of $-\delta B_i/B_s$ match those of LES rather well, increasing in time much like the LES $-\delta B_i/B_s$ does. Since the Sorbjan (2004) parameterization consistently underpredicted the entrainment flux ratio in our initial tests, we elected to double the value of c_H when evaluating (31) against the LES data. The results for the doubled c_H are shown in our figures.

2) GC CASE

The predictions of the ZOM-based parameterizations T73, D82, and BG94 are probably better suited to be tested against the GC case simulations because of the strong surface shear in those cases. All these parameterizations show enhanced entrainment flux ratios in Fig. 4a, but the predicted entrainment flux ratios are a bit larger than those derived from LES. The qualitative time tendency of the parameterized entrainment flux ratios reproduces the behavior of the LES-retrieved ratios reasonably well, with very large ratios early in the simulation and rapidly decreasing ratios soon thereafter, with the ratios approaching nearly constant values late in the simulations. As the simulation proceeds, the larger z_i in the convective velocity scale $w_* = (B_s z_i)^{1/3}$ becomes dominant over the effects of the surface shear (u_*) in (24), so (24) may reasonably well mimic the simulated behavior of $-B_{i0}/B_s$, as appears to be the case in Fig. 4a. Although the results of Part I testify the entrainment depends directly on entrainment zone shear and not surface shear, the surface shear does have a direct effect on the mixed layer velocity (as was discussed in Part I), which partly determines the entrainment zone shear, so equations like (24) seem to model the qualitative behavior of entrainment (such as decreasing entrainment flux ratios with time) rather well for the GC cases.

Similar overpredictions of the entrainment flux ratio

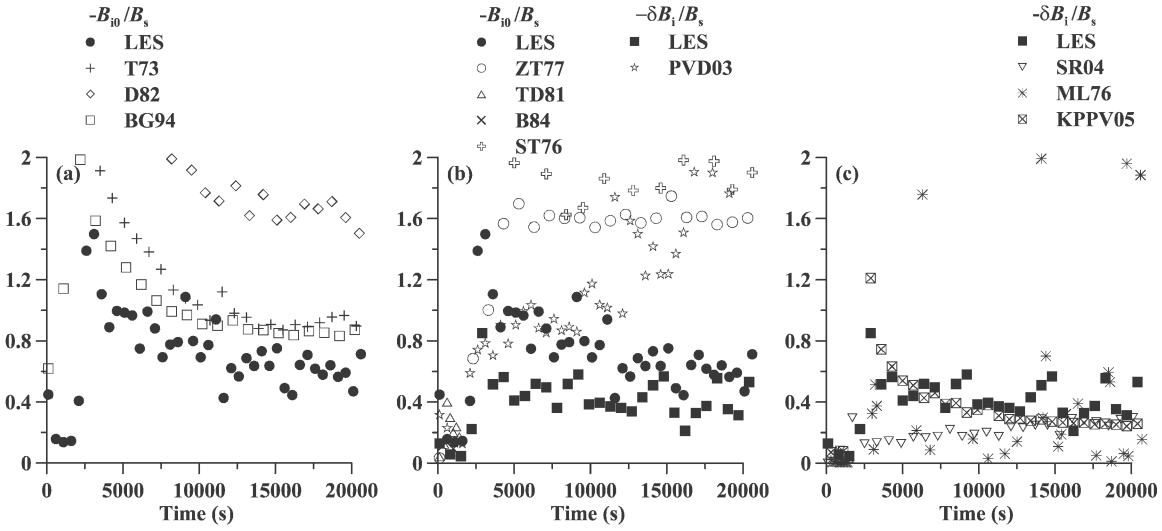

FIG. 4. Entrainment flux ratio predicted for the GC case with $\partial\theta/\partial z = 0.003$ K m^{-1} and $Q_s = 0.03$ K m s^{-1}. For notation, see Fig. 3.

are seen in Fig. 4b, where the qualitative time behavior of the parameterized entrainment flux ratios differs from LES. The ZT77 and ST76 parameterizations predict nearly constant ratios between 1.6 and 2, and the P03 parameterization predicts a steadily increasing $\delta B_i/B_s$ that does not behave similarly to the LES-derived $\delta B_i/B_s$. Again, the B84 parameterization does not predict realistic entrainment flux ratios; its denominator becomes less than zero because of the large C_P it employs. The TD81 parameterization also goes off the scale used in the figure.

Among parameterizations shown in Fig. 4c, both the SR04 and K05 parameterizations describe the LES-predicted $\delta B_i/B_s$ in a realistic manner, although the SR04 parameterization provides slightly lower values of the entrainment ratio than the LES does. The K05 parameterization produces large $\delta B_i/B_s$ early on, followed by a gradual decrease of the predicted entrainment flux ratios over the remainder of the simulation. This seems to agree with the qualitative behavior of $\delta B_i/B_s$ in the simulations. The K05-assumed fraction C_P of entrainment zone shear-generated TKE available for entrainment is higher than the value of C_P obtained from the LES in Part I. Nevertheless, the K05 parameterization still predicts the simulated $\delta B_i/B_s$ rather well. It is uncertain whether this is the result of insensitivity to C_P or the result of a mutual cancellation of errors arising from an excessive value of C_P combined with the confusing expression 0.5 $(\Delta u_1 + \Delta v_1)$ for the velocity increment across the entrainment zone. The ML76 parameterization again appears to suffer from its simplification of the TKE equation and its dissipation assumptions. Consequently, the denominator fluctuates around zero, and the parameterization predicts ratios that considerably fluctuate over the course of the simulation.

b. $\partial\theta/\partial z = 0.01$ K m^{-1} and $Q_s = 0.1$ K m s^{-1}

1) GS CASES

In CBLs, which are more dominated by buoyancy effects both in terms of buoyancy production of TKE and the potential temperature stratification in the free atmosphere, the predictions of entrainment by some of the parameterizations fall in line with the simulated entrainment flux ratios. However, Fig. 5a shows that the surface-shear-only parameterizations still underpredict the entrainment flux ratio relative to LES because they do not account for the entrainment zone shear, which is the dominant entrainment-enhancement factor in this case.

Again, the parameterizations with entrainment zone shear show a stronger dependence of the entrainment flux ratio on the shear. With strong stratification, the B84 parameterization is less subject to the problems associated with the denominator hovering around zero, and its predictions of $-B_{i0}/B_s$ are on the scale displayed in the figure, but the values are still much higher than the LES predicts. This is a further testament to the underpredicted dissipation of shear-produced TKE. The parameterized $-B_{i0}/B_s$ from TD81 matches the LES values more closely than in Fig. 3b, but the predicted entrainment ratio values are again larger than the simulated ones. The LES results discussed in Part I suggest that the surface shear-generated TKE does not have a direct influence on the entrainment and, if the effects of both the surface shear and entrainment zone shear are included in the entrainment equation, the

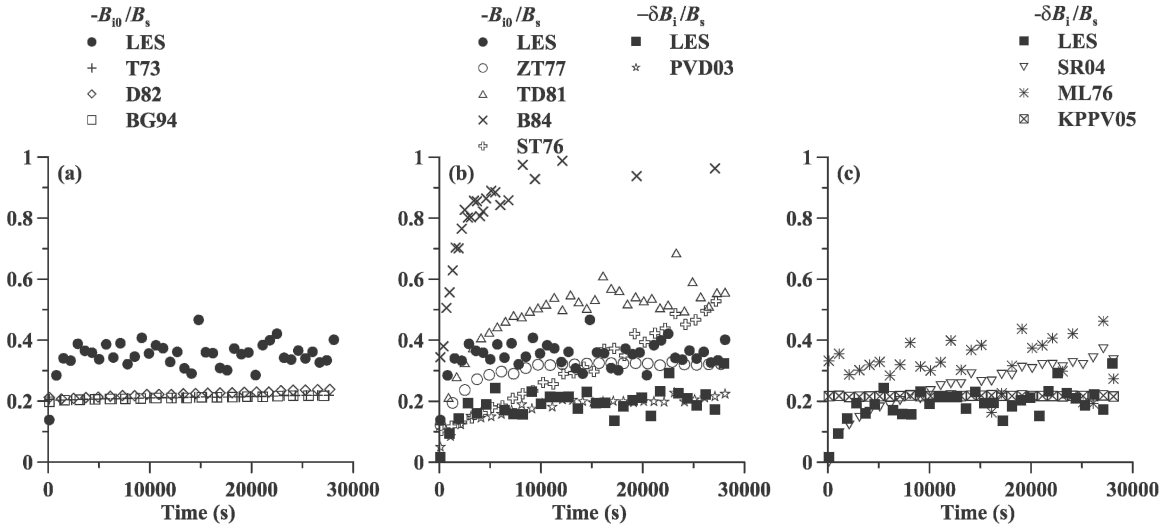

FIG. 5. Entrainment flux ratio predicted for the GS case with $\partial\theta/\partial z = 0.010$ K m^{-1} and $Q_s = 0.1$ K m s^{-1}. For notation, see Fig. 3.

equation tends to overpredict the entrainment. However, the ZT77 and P03 parameterized entrainment flux ratios match their LES counterparts very well in this case.

The ST76 parameterization performs reasonably well overall, but it predicts a steady increase of the entrainment ratio, whereas the entrainment flux ratios from LES tend to level off with time. This could partially be a result of steadily increasing surface shear during the simulation. Moreover, in (25), the numerator of the entrainment zone shear term is cubic in $|\Delta\mathbf{u}|$, and there is B_s in the denominator, which remains constant with time in this study. On the other hand, in (21), the entrainment zone shear term, proportional to the square of velocity jump, is divided by a Δb that increases with time in the simulations. So the entrainment flux ratios parameterized by (21) level off with time as they do in the simulations, whereas the ST76 parameterization is unable to model this behavior.

Of all the parameterizations shown in Fig. 5c, the SR04 parameterization of the entrainment flux ratio best matches the simulated ratio $-\delta B_i/B_s$. Remarkably, it accomplishes this without taking into account the effects of surface shear, which is a further indication that surface shear TKE production may not be directly important for the entrainment enhancement. The ML76 parameterization also performs reasonably well, but it overpredicts the ratio a little bit just like the K05 parameterization does. The K05 parameterization matches LES $-\delta B_i/B_s$ rather well, but the values do not change as much over the simulation as the LES values do.

2) GC CASES

The behavior of the entrainment flux ratios in Fig. 6a matches LES entrainment flux ratios more closely than in Fig. 4a and, as is the case in Fig. 5a, the TKE generation and consumption is dominated by the buoyancy forcing. However, the relative differences between LES and the parameterizations are qualitatively the same as those shown in Fig. 4a. In particular, the D82 predictions of $-B_{i0}/B_s$ are nearly double the simulated $-B_{i0}/B_s$. The increased dominance of buoyancy-related production of TKE in this case, compared to that in section 4a(2), allows (23), with a larger w_*, to predict a lower entrainment flux ratio, matching the LES ratio more closely.

In Fig. 6b, the P03 parameterization most closely predicts the value of the simulated entrainment flux ratio in the overall sense, although the predicted time dependence is somewhat different from the simulated time dependence. The P03-predicted entrainment flux ratios remain nearly constant, while the simulated ratios decrease slightly. The P03 expression has a smaller value of A, so the decrease of the ratio w_m^3/w_*^3 with time is not as significant as it is in the other parameterizations. It also has a larger C_T in the temporal term, which acts to decrease modeled entrainment flux ratios at early stages of CBL evolution when dz_i/dt is large. The ST76 and TD81 parameterizations overpredict $-B_{i0}/B_s$, with the TD81 parameterization being off-scale in the first half of the simulation and decreasing to $-B_{i0}/B_s < 2$ in the second half. The ST76-parameterized $-B_{i0}/B_s$ steadily increases during the run, again due to the entrainment zone shear term being cubic and not divided by Δb.

In Fig. 6c, the SR04 parameterization most closely matches the simulated entrainment flux ratio $-\delta B_i/B_s$, although the values are a little low early in the simulation and slightly larger than the LES values by the end.

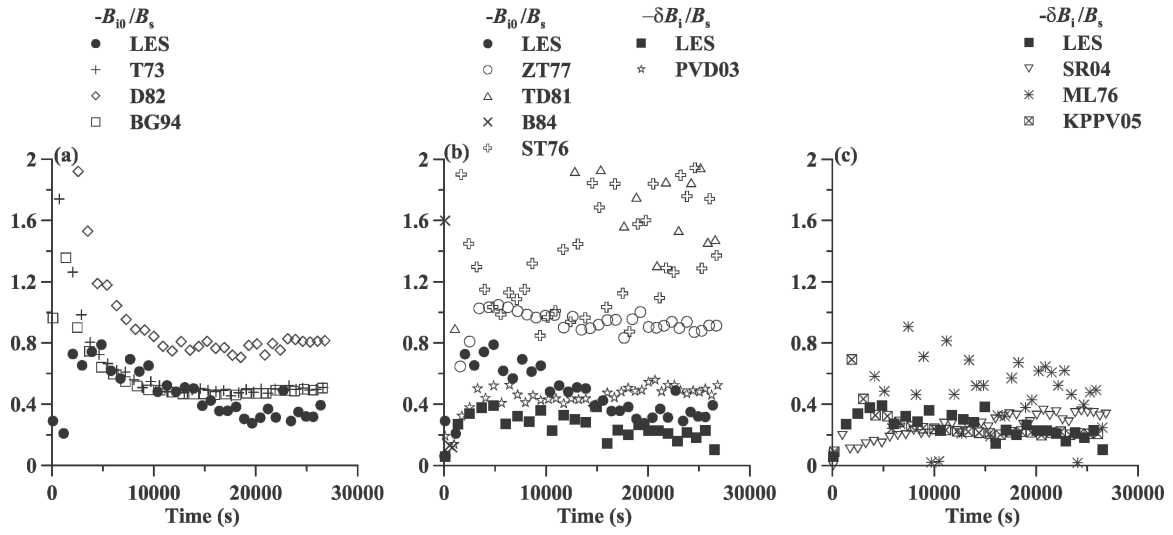

FIG. 6. Entrainment flux ratio predicted for the GC case with $\partial\theta/\partial z = 0.010$ K m^{-1} and $Q_s = 0.1$ K m s^{-1}. For notation, see Fig. 3.

The ML76-parameterized entrainment flux ratios also compare reasonably well with the simulated ratios but are a little high. Finally, the K05-predicted ratios are, again, a little higher than the LES ratios at the very earliest stages of the simulation, but they match the LES ratios quite closely over the remainder of the simulation. Perhaps some of the excessively large ratios early in the simulation are due to the fact that u_* appears twice in (29): once in the term associated with A_{2K} and again in the term with A_{3K}. The surface friction velocity u_* does not appear in the SR04 parameterization and, given that most of the surface-generated TKE is dissipated locally (Lenschow 1970, 1974; Deardorff and Willis 1982; Moeng and Sullivan 1994; Part I), it brings us to the idea that near-surface shear production may be neglected in the TKE integral budget (entrainment) equation whenever the entrainment zone shear is included in the parameterization.

c. $\partial\theta/\partial z = 0.01$ K m^{-1} and $Q_s = 0.3$ K m s^{-1}

1) GS CASES

Figure 7 presents entrainment ratios for the GS cases in which the buoyancy production of TKE is dominant over the shear production of TKE. The parameterization outputs do not differ much from one another be-

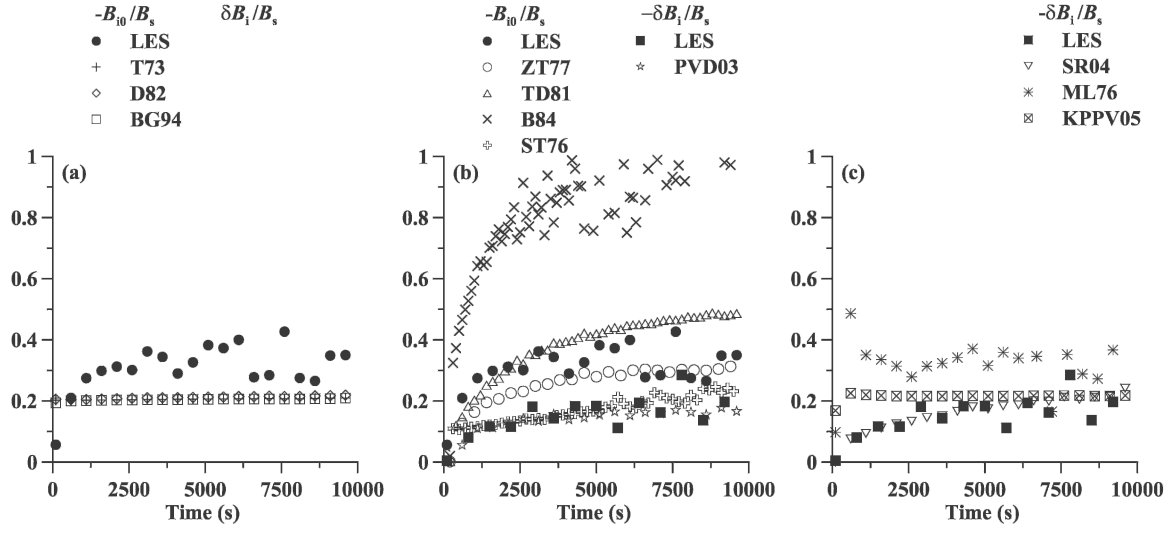

FIG. 7. Entrainment flux ratio predicted for the GS case with $\partial\theta/\partial z = 0.010$ K m^{-1} and $Q_s = 0.3$ K m s^{-1}. For notation, see Fig. 3.

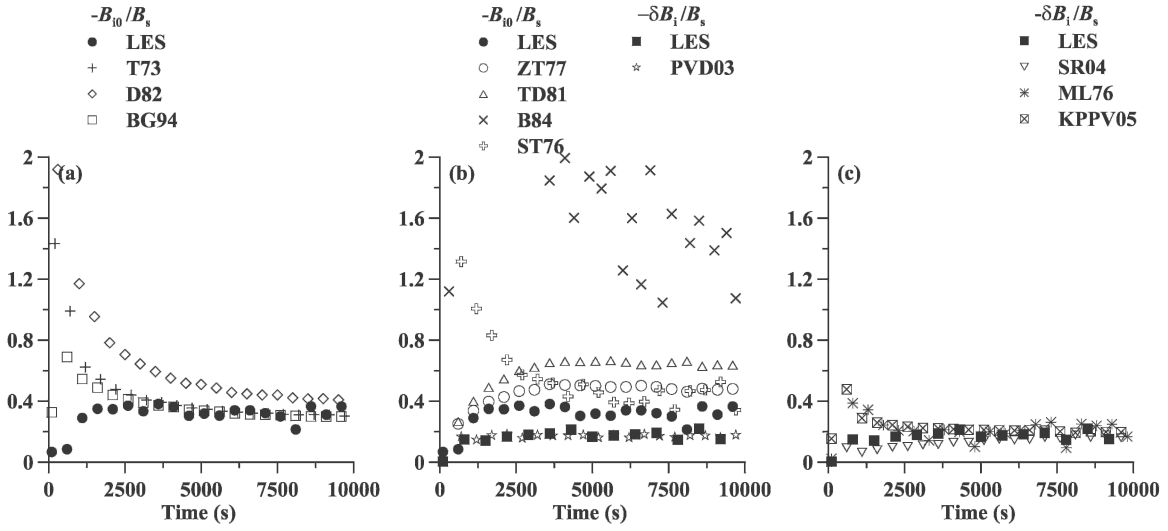

FIG. 8. Entrainment flux ratio predicted for the GC case with $\partial\theta_s/\partial z = 0.010$ K m^{-1} and $Q_s = 0.3$ K m s^{-1}. For notation, see Fig. 3.

cause the free-atmospheric stratification is larger in CBL cases presented in Figs. 5 and 7 than in the ones shown in Fig. 3. The value of Δb is therefore larger, acting to compensate the shear term, and a larger Δb suppresses the CBL growth in general (Sorbjan 1996a,b). Since the stratification is the same in Figs. 5 and 7 and the friction velocity is relatively small in the GS cases (preventing the ratio w_m^3/w_*^3 from changing much, even though w_*^3 increases with the larger B_s), most of the entrainment parameterizations in Figs. 5b and 5c and in Figs. 7b and 7c are not much different because the denominator of (23) has approximately the same value in both cases. This small variability of the parameterized ratios matches the simulated change in the behavior of $-B_{i0}/B_s$ rather well. The ST76-parameterized ratios, however, are smaller in Fig. 7b compared to Fig. 5b because of the larger B_s in the denominators of both shear terms. Therefore, the ST76 parameterization does not predict the simulated change in entrainment flux ratio between Figs. 5b and 7b like the parameterizations of the form (23) do.

2) GC CASES

In the GC cases, the ratio w_m^3/w_*^3 decreases with increasing B_s, so the surface-shear-only parameterizations produce smaller entrainment flux ratios (cf. Fig. 8a with Fig. 6a). For the ZOM parameterizations, which include both shears, there are two major factors responsible for the differences between entrainment ratios in Fig. 8b and Fig. 6b. First, because B_s is larger in the CBL cases shown in Fig. 8b, w_m^2 is also larger, resulting in a larger temporal term in the denominator of (21). Also, because of the more rapidly growing CBL and active entrainment of momentum in the cases shown in Fig. 8b, the mixed layer velocity more closely matches the free-atmospheric velocity, and the entrainment zone shear term is slightly smaller. These two effects reduce the chances of the denominator becoming close to zero. Secondly, the smaller values of w_m^3/w_*^3 further decrease the parameterized entrainment flux ratios; these ratios are smaller in Fig. 8b than in Fig. 6b.

With the exception of the B84 parameterization, which uses $C_P = 1$, all parameterized $-B_{i0}/B_s$ values fall close the simulated range of $-B_{i0}/B_s$ in Fig. 8b. In general, the parameterizations perform rather well in the buoyancy-dominated CBLs because the value $C_1 = 0.2$ is rather well established for such CBLs, and the relative influence of the shear generation of TKE, whose effects on entrainment are less well understood, is smaller in this case. The poor performance of B84 relative to the other parameterizations, when compared against LES data, is a strong indicator that $C_P = 1$ is an overestimation, and therefore the dissipation of entrainment zone shear-generated TKE is probably larger than has been assumed in previous studies.

The ST76-parameterized entrainment flux ratios decrease proportionally with the increase in B_s between Fig. 6b and Fig. 8b (a factor of 3), and the cubic entrainment zone shear term is greatly affected by the small decrease in entrainment zone shear as well. So overall, the performance of the ST76 parameterization is dramatically affected by these changes. The SR04-predicted ratios decrease a bit as well (see Fig. 8c) since the increase in $\mathrm{Ri}_{\delta b}$ seems to be more significant than the increase in w_*^2, see (31). The FOM-based parameterizations are affected by the increased B_s and slightly

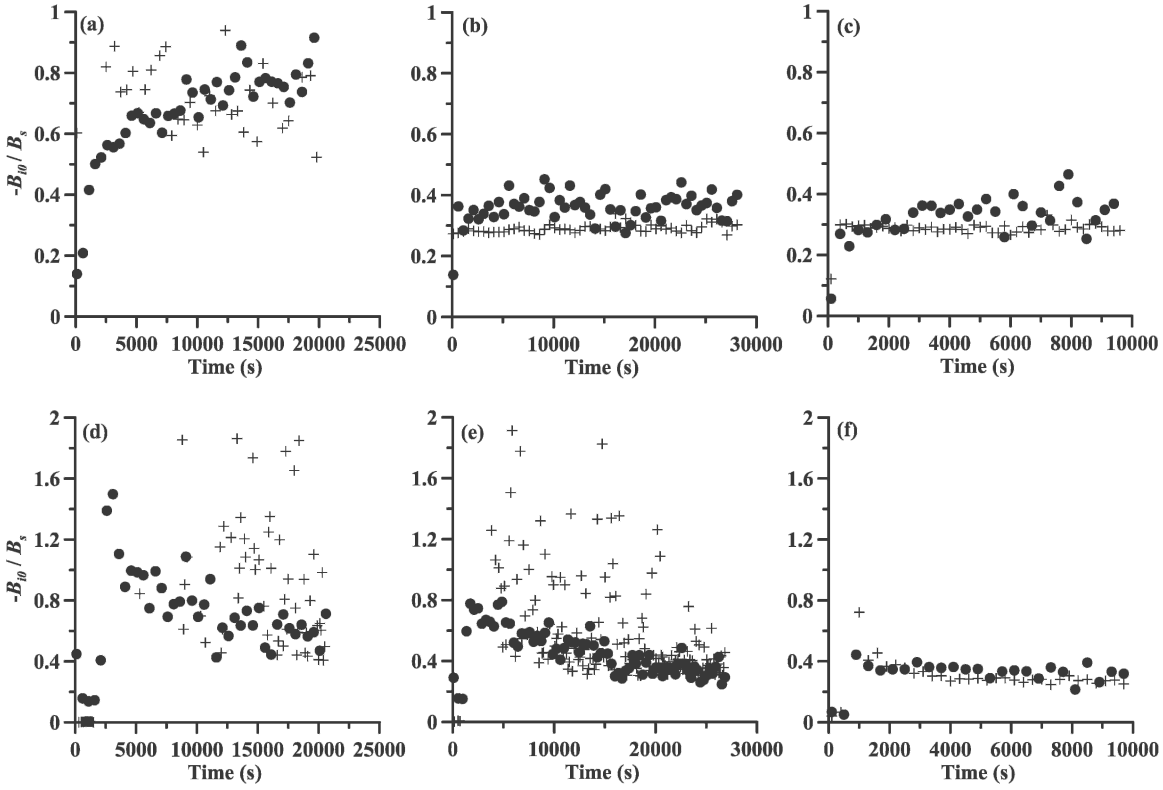

FIG. 9. Comparison between entrainment flux ratio predicted as a result of this study (crosses) and LES (solid dots) for the GS cases with (a) $\partial\theta/\partial z = 0.003$ K m^{-1} and $Q_s = 0.03$ K m s^{-1}; (b) $\partial\theta/\partial z = 0.010$ K m^{-1} and $Q_s = 0.1$ K m s^{-1}; (c) $\partial\theta/\partial z = 0.010$ K m^{-1} and $Q_s = 0.3$ K m s^{-1}; GC cases with (d) $\partial\theta/\partial z = 0.003$ K m^{-1} and $Q_s = 0.03$ K m s^{-1}; (e) $\partial\theta/\partial z = 0.010$ K m^{-1} and $Q_s = 0.1$ K m s^{-1}; and (f) $\partial\theta/\partial z = 0.010$ K m^{-1} and $Q_s = 0.3$ K m s^{-1}.

decreased entrainment zone shear in the same manner as the ZOM parameterizations are.

d. Evaluations with new values of constants

Finally, we evaluate (23) with new constants chosen from the results of the LES analyses in Part I. For both the GS and GC cases with $\partial\theta/\partial z = 0.003$ K m^{-1} (Fig. 9a) and $Q_s = 0.03$ K m s^{-1} (Fig. 9d), the new constants provide a better prediction of the entrainment flux ratio, compared to predictions with larger values of A, C_t, and C_P. Values for the GS case match the LES entrainment flux ratio rather well, but in the GC cases there is still some overprediction of the ratio. In both cases, the parameterization still displays great sensitivity to the values of the integral parameters of entrainment retrieved from LES and, therefore, has a lot of scatter.

With $\partial\theta/\partial z = 0.010$ K m^{-1} and $Q_s = 0.1$ K m s^{-1}, there is somewhat less scatter, like in the earlier considered entrainment predictions for CBLs growing in the more stably stratified free atmosphere (see section 4b and Figs. 5b and 6b). Nevertheless, there is still some overprediction of the ratio for the GC case (Fig. 9e), although a majority of the data points fall relatively close to the LES-retrieved entrainment flux ratios. In the GS case (Fig. 9b), the parameterized entrainment flux ratio values are actually somewhat smaller than those retrieved from LES. Overall, for both GS and GC cases, the parameterization performs reasonably well.

With $\partial\theta/\partial z = 0.010$ K m^{-1} and $Q_s = 0.3$ K m s^{-1} (Figs. 9c and 9f), the parameterization with new constants performs best. One must keep in mind that these cases are most buoyancy-dominated, and one can expect errors in the quantification of the shear to be masked, to some extent, by the buoyancy domination. Nevertheless, one can see the general improvement in the predictions of $-B_{i0}/B_s$ over similar parameterizations of the form (23) when comparing Figs. 9c and 9f with Figs. 7b and 8b.

Overall, the improved predictions of $-B_{i0}/B_s$ indicate the use of (23) as the form of the TKE equation, with lower values of A, C_t, and C_P, along with (5), (6), and (7) as equations to describe the parameters of entrainment Δb, Δu, and Δv, should quantify the effects of shear on the evolution of the CBL rather well. In fact, when these equations are integrated, the output (not shown) agrees favorably well with LES in most cases,

but there are still some cases that present some difficulty in matching the integration output with the LES output. This may be the result of deficiencies in the ZOM representation of the sheared CBL structure. Preliminary tests of equations developed using the FOM representation show some improvement over the ZOM-based equations. A more thorough investigation of the utility of FOM-based equations for parameterization of entrainment in sheared CBLs will be saved for future study.

5. Summary and conclusions

The reported study has examined the behavior of the numerical models of entrainment in sheared CBLs by comparing the bulk model parameterizations for the buoyancy flux at the CBL top with LES data. The tests of the integral budget-based entrainment parameterizations suggested to date show that most of them overestimate entrainment in CBLs with strong shear. It may be argued that the shear in the numerically simulated CBL cases was rather strong. However, the CBL cases selected for comparison with bulk models were specifically designed to make the relative effects of shear more prominent and to make the tests of the entrainment equations more severe.

Perhaps the most important conclusion reached in the present analysis concerns the shear-produced TKE that is available for entrainment. It was found to be lower than has been reported in earlier studies, both for the entrainment zone shear-produced TKE and for the surface layer shear-produced TKE. For the entrainment zone shear, the fraction C_P in (23) should be lowered from the commonly used value of 0.7 to the value of 0.4 retrieved from the LES data in Part I. It also appears from Part I that essentially all of the surface-generated TKE is dissipated in the lower portion of the CBL so that the value of A can be set to zero in parameterizations such as (23). Therefore, within the ZOM methodological framework, the use of (23) as the form of the TKE equation with the values of $A = 0$, $C_T = 0$, and $C_P = 0.4$, along with (5), (6), and (7) as the momentum and buoyancy integral balance equations, appear to quantify the effects of shear on the evolution of the CBL rather well.

Nevertheless, our results also show that the parameterizations that include only the surface layer shear (and exclude the entrainment zone shear) perform rather well against the simulated GC cases since, in these cases, the surface friction velocity acts as a proxy for the entrainment zone shear effect, provided the surface layer shear is relatively strong. It merely appears that the value of A needs to be reduced somewhat in (24). In the GS cases, where entrainment zone shear is large and surface layer shear is very weak, the parameterizations accounting only for surface shear perform poorly. It should be noted, however, that with their very strong geostrophic shear, the GS cases can be considered less representative of typical atmospheric conditions than the GC cases are.

In our final tests of (23), we have chosen to omit the TKE spinup term entirely, and the results of the tests show that it is generally not an important term for the CBL cases included in the present study. Probably, also, the overall meaning of this term has to be reconsidered, given the findings reported in the present paper as well as in Fedorovich et al. (2004a,b). It is still possible that the term may turn out to be significant in CBL cases strongly affected by nonstationarity of the TKE integral budget.

Provided that Kelvin–Helmholtz instabilities appear to be an inherent feature of convective entrainment in the presence of wind shears, as our and other LES show (see, e.g., Kim et al. 2003), any Richardson-number-dependent entrainment equation in which the Richardson number is local to the entrainment zone (versus a bulk Ri for the whole CBL) would seem to be most suited to predict the growth dynamics of the sheared CBL. In bulk models of the CBL, this local Richardson number dependence can be represented by including an interfacial layer of linearly changing buoyancy and velocity at the top of the CBL, as implied in the FOM-based parameterizations, and using the Richardson number to relate the buoyancy and momentum increments across this layer. The results of section 4 indicate that such a representation of the entrainment zone structure improves the ability of bulk parameterizations to model the simulated entrainment flux ratios in the sheared CBL cases. It is possible, however, that the higher-order terms neglected while developing some FOM-based entrainment parameterizations may remain important for the strongly sheared CBLs, and the absence of these terms might also be affecting the results of the presented analysis. The issues surrounding the neglected terms will be addressed in future work.

The entrainment equations that are derived by adhering strictly to the ZOM and FOM methodology contain the entrainment zone shear as a negative-sign term in the denominator, which often makes the denominator zero or negative. Such apparently poor mathematical formulation of the problem may be the result of insufficient physical hypotheses, such as the lack of spinup terms associated with shear-generated TKE or underestimated dissipation of entrainment zone shear-generated TKE. The strictly ZOM-based parameterizations modeled the qualitative temporal behavior of the

entrainment flux ratio better than parameterizations that circumvent the problem of the negative sign term in the denominator. Likewise, traditional ZOM parameterizations tended to reproduce the sensitivity of entrainment to surface buoyancy flux B_s and free-atmospheric stratification better than the deviant models.

Acknowledgments. This work has been supported by the National Science Foundation within Grant ATM-0124068. The first author would like to thank members of his Ph.D. advisory committee: Charles A. Doswell III, Brian Fiedler, Randall Kolar, Douglas Lilly, and Alan Shapiro for their insightful comments on guidance of this work. Gratitude is also extended to Si-Wan Kim and Don Lenschow of the Mesoscale and Microscale Meteorology division of the National Center for Atmospheric Research and David Pino of the Institut d'Estudis Espacials de Catalunya and Departament de Fisica Aplicada, Universitat Politecnica de Catalunya, Barcelona (Spain), as well as Jordi Vilà-Guerau de Arellano of the Meteorology and Air Quality Group, Wageningen University (Netherlands) for discussions regarding ZOM- and FOM-based entrainment equations. The authors are grateful to three anonymous reviewers for their constructive suggestions on improvement of the manuscript and to the University of Oklahoma School of Meteorology for helping fund the publication of this manuscript.

REFERENCES

Ball, F. K., 1960: Control of inversion height by surface heating. *Quart. J. Roy. Meteor. Soc.,* **86,** 483–494.

Batchvarova, E., and S.-E. Gryning, 1991: Applied model for the growth of the daytime mixed layer. *Bound.-Layer Meteor.,* **56,** 261–274.

——, and ——, 1994: An applied model for the height of the daytime mixed layer and the entrainment zone. *Bound.-Layer Meteor.,* **71,** 311–323.

Betts, A. K., 1973: Non-precipitating cumulus convection and its parameterization. *Quart. J. Roy. Meteor. Soc.,* **99,** 178–196.

——, 1974: Reply to comment on the paper "Non-precipitating cumulus convection and its parameterization." *Quart. J. Roy. Meteor. Soc.,* **100,** 469–471.

Boers, R., E. W. Eloranta, and R. L. Coulter, 1984: Lidar observations of mixed layer dynamics: Tests of parameterized entrainment models of mixed layer growth rate. *J. Climate Appl. Meteor.,* **23,** 247–266.

Carson, D. J., 1973: The development of a dry inversion-capped convectively unstable boundary layer. *Quart. J. Roy. Meteor. Soc.,* **99,** 450–467.

Conzemius, R., and E. Fedorovich, 2004: Numerical models of entrainment into sheared convective boundary layers evaluated through large eddy simulations. Preprints, *16th Symp. on Boundary Layers and Turbulence,* Portland, ME, Amer. Meteor. Soc., CD-ROM, P5.6.

——, and ——, 2006: Dynamics of sheared convective boundary layer entrainment. Part I: Methodological background and large eddy simulations. *J. Atmos. Sci.,* **63,** 1151–1178.

Deardorff, J. W., 1970: Convective velocity and temperature scales for the unstable planetary boundary layer and for Raleigh convection. *J. Atmos. Sci.,* **27,** 1211–1213.

——, and G. E. Willis, 1982: Dependence of mixed-layer entrainment on shear stress and velocity jump. *J. Fluid Mech.,* **115,** 123–140.

Driedonks, A. G. M., 1982: Models and observations of the growth of the atmospheric boundary layer. *Bound.-Layer Meteor.,* **23,** 283–306.

Fedorovich, E., 1995: Modeling the atmospheric convective boundary layer within a zero-order jump approach: An extended theoretical framework. *J. Appl. Meteor.,* **34,** 1916–1928.

——, 1998: Bulk models of the atmospheric convective boundary layer. *Buoyant Convection in Geophysical Flows,* E. J. Plate et al., Eds., Kluwer, 265–290.

——, R. Conzemius, and D. Mironov, 2004a: Convective entrainment into a shear-free, linearly stratified atmosphere: Bulk models reevaluated through large eddy simulations. *J. Atmos. Sci.,* **61,** 281–295.

——, ——, and A. Shapiro, 2004b: Nonstationarity of convective boundary layer growth in a heterogeneously stratified, shear-free atmosphere. Preprints, *16th Symp. on Boundary Layers and Turbulence,* Portland, ME, Amer. Meteor. Soc., CD-ROM, P7.9.

——, and Coauthors, 2004c: Entrainment into sheared convective boundary layers as predicted by different large eddy simulation codes. Preprints, *16th Symp. on Boundary Layers and Turbulence,* Portland, ME, Amer. Meteor. Soc., CD-ROM, P4.7.

Garratt, J. R., 1992: *The Atmospheric Boundary Layer*. Cambridge University Press, 316 pp.

Kato, H., and O. M. Phillips, 1969: On the penetration of a turbulent layer into stratified fluid. *J. Fluid Mech.,* **37,** 643–655.

Kim, S.-W., S.-U. Park, and C.-H. Moeng, 2003: Entrainment processes in the convective boundary layer with varying wind shear. *Bound.-Layer Meteor.,* **108,** 221–245.

Lenschow, D. H., 1970: Airplane measurements of planetary boundary layer structure. *J. Appl. Meteor.,* **9,** 874–884.

——, 1974: Model of the height variation of the turbulence kinetic energy budget in the unstable planetary boundary layer. *J. Atmos. Sci.,* **31,** 465–474.

Lilly, D. K., 1968: Models of cloud-topped mixed layers under a strong inversion. *Quart. J. Roy. Meteor. Soc.,* **94,** 292–309.

Mahrt, L., and D. H. Lenschow, 1976: Growth dynamics of the convectively mixed layer. *J. Atmos. Sci.,* **33,** 41–51.

Moeng, C.-H., and P. P. Sullivan, 1994: A comparison of shear- and buoyancy-driven planetary boundary layer flows. *J. Atmos. Sci.,* **51,** 999–1022.

Pino, D., J. V.-G. de Arellano, and P. J. Duynkerke, 2003: The contribution of shear to the evolution of a convective boundary layer. *J. Atmos. Sci.,* **60,** 1913–1926.

Price, J. F., C. N. K. Mooers, and J. C. van Leer, 1978: Observation and simulation of storm-induced mixed layer deepening. *J. Phys. Oceanogr.,* **8,** 582–599.

Sorbjan, Z., 1996a: Numerical study of penetrative and "solid lid" nonpenetrative convective boundary layers. *J. Atmos. Sci.,* **53,** 101–112.

——, 1996b: Effects cause by varying the strength of the capping

inversion based on a large eddy simulation model of the shear-free convective boundary layer. *J. Atmos. Sci.,* **53,** 2015–2024.

——, 2004: Large-eddy simulation of the baroclinic mixed layer. *Bound.-Layer Meteor.,* **112,** 57–80.

Stull, R. B., 1973: Inversion rise model based on penetrative convection. *J. Atmos. Sci.,* **30,** 1092–1099.

——, 1976a: The energetics of entrainment across a density interface. *J. Atmos. Sci.,* **33,** 1260–1267.

——, 1976b: Internal gravity waves generated by penetrative convection. *J. Atmos. Sci.,* **33,** 1279–1286.

——, 1976c: Mixed-layer depth model based on turbulent energetics. *J. Atmos. Sci.,* **33,** 1268–1278.

Sullivan, P., C.-H. Moeng, B. Stevens, D. H. Lenschow, and S. D. Mayor, 1998: Structure of the entrainment zone capping the convective atmospheric boundary layer. *J. Atmos. Sci.,* **55,** 3042–3064.

Tennekes, H., 1973: A model for the dynamics of the inversion above a convective boundary layer. *J. Atmos. Sci.,* **30,** 558–567.

——, and A. G. M. Driedonks, 1981: Basic entrainment equations for the atmospheric boundary layer. *Bound.-Layer Meteor.,* **20,** 515–531.

vanZanten, M. C., P. G. Duynkerke, and J. W. M. Cuijpers, 1999: Entrainment parameterization in convective boundary layers. *J. Atmos. Sci.,* **56,** 813–828.

Zeman, O., and H. Tennekes, 1977: Parameterization of the turbulent energy budget at the top of the daytime atmospheric boundary layer. *J. Atmos. Sci.,* **34,** 111–123.

Zilitinkevich, S. S., 1991: *Turbulent Penetrative Convection.* Avebury Technical, 179 pp.